Title: Multilayer OMIC data in medullary thyroid carcinoma identifies the STAT3 pathway as a potential therapeutic target in *RET*^{M918T} tumors.

Running title: Genomic integration in medullary thyroid carcinoma.

Key words: 27K array methylation, MTC, RET, RAS, OMIC data integration.

Authors: Veronika Mancikova[1*], Cristina Montero-Conde[1*], Javier Perales-Paton[2], Agustin Fernandez[3], María Santacana[4], Karolina Jodkowska[5], Lucia Inglada-Pérez[1,6], Esmeralda Castelblanco[7,8], Salud Borrego[9], Mario Encinas[4], Xavier Matias-Guiu[4,10], Mario Fraga[3], Mercedes Robledo[1,6]

*These authors contributed equally to the work.
1-Hereditary Endocrine Cancer Group, Spanish National Cancer Research Centre (CNIO), Madrid, Spain
2-Translational Bioinformatics Unit, Clinical Research Program, Spanish National Cancer Research Centre (CNIO), Madrid, Spain
3-Cancer Epigenetics Laboratory, Institute of Oncology of Asturias (IUOPA), HUCA, University of Oviedo, Asturias, Spain
4-Department of Endocrinology and Nutrition, University Hospital Arnau de Vilanova, IRBLLEIDA, Lleida, Spain
5-DNA Replication Group, Spanish National Cancer Research Centre (CNIO), Madrid, Spain
6-ISCIII Center for Biomedical Research on Rare Diseases (CIBERER), Madrid, Spain
7-Department of Endocrinology and Nutrition, Germans Trias i Pujol Hospital, Health Sciences Research Institute of the "Germans Trias i Pujol" Foundation (IGTP), Badalona, Spain
8-Centre for Biomedical Research on Diabetes and Associated Metabolic Diseases (CIBERDEM), ISCIII, Spain
9-Hospital Virgen del Rocío, Sevilla
10-Department of Pathology, Hospital Universitari de Bellvitge, IDIBELL, Barcelona

Corresponding author:

Dr. Mercedes Robledo, Spanish National Cancer Center (CNIO), Calle Melchor Fernandez Almagro 3, 28029 Madrid, Spain. Tel. +34 917 328 000; Fax. +34 912 246 972; mrobledo@cnio.es

Word count: 4616
Total number of tables and figures: 5 figures
DISCLOSURE OF POTENTIAL CONFLICT OF INTEREST

No competing interests exist.

GRANT SUPPORT

This work was supported by the *Fondo de Investigaciones Sanitarias* (FIS) project PI14/00240 and the *Comunidad de Madrid* (Grant S2011/BMD-2328 TIRONET) to MR. LI-P is supported by the *Centro de Investigacion Biomédica en Red de Enfermedades Raras* (CIBERER). VM was supported by a predoctoral fellowship from the "la Caixa"/CNIO international PhD programme. CM-C is supported by a postdoctoral fellowship from the *Fundación AECC*.

STATEMENT OF TRANSLATIONAL RELEVANCE

Medullary thyroid carcinoma (MTC) is a rare disease with few genetic drivers that, when diagnosed at advanced stage, remains incurable. Due to its rarity, its genomic dissection has not been comprehensively explored. This multilayer genomic study, considering the transcriptome, miRNome and methylome, is the first of its kind and has uncovered genes negatively regulated by methylation. Functional annotation enrichment analysis identified the JAK/Stat pathway as a specific hallmark of *RET*^{M918T}-bearing MTCs. *In vitro* studies with MTC cell models point to a *RET*^{M918T} genetic class-specific proliferative dependency on STAT3 activity. Remarkably, the inhibition of STAT3 increases the sensitivity of *RET*^{M918T}-bearing MTC cells to the FDA-approved RET inhibitor Vandetanib. This combinational treatment could potentially overcome the adverse effects encountered in clinical practice when Vandetanib monotherapy is applied.

ABSTRACT

Purpose: Medullary thyroid carcinoma (MTC) is a rare disease with few genetic drivers, and the etiology specific to each known susceptibility mutation remains unknown. Exploiting multilayer genomic data, we focused our interest on the role of aberrant DNA methylation in MTC development.

Experimental design: We performed genome-wide DNA methylation profiling assessing >27,000 CpGs in the largest MTC series reported to date, comprising 48 molecularly characterized tumors. mRNA and miRNA expression data was available for 33 and 31 tumors, respectively. Two human MTC cell lines and 101 paraffin-embedded MTCs were used for validation.

Results: The most distinctive methylome was observed for *RET*^{M918T}-related tumors. Integration of methylation data with mRNA and miRNA expression data identified genes negatively regulated by promoter methylation. These *in silico* findings were confirmed *in vitro* for *PLCB2*, *DKK4*, *MMP20* and miR-10a, -30a and -200c. The mutation-specific aberrant methylation of *PLCB2*, *DKK4* and *MMP20* was validated in 25 independent MTCs by bisulfite pyrosequencing. The methylome and transcriptome data underscored JAK/Stat pathway involvement in *RET*^{M918T} MTCs. Immunostaining (IHC) for the active form of signaling effector STAT3 was performed in a series of 101 MTCs. As expected, positive IHC was associated with *RET*^{M918T}-bearing tumors (p-value<0.02). Pharmacological inhibition of STAT3 activity increased the sensitivity to Vandetanib of the *RET*^{M918T}-positive MTC cell line, MZ-CRC-1.

Conclusions: Multilayer OMIC data analysis uncovered methylation hallmarks in genetically defined MTCs and revealed JAK/Stat signaling effector STAT3 as a potential therapeutic target for the treatment of *RET*^{M918T} MTCs.

INTRODUCTION

Medullary thyroid carcinoma (MTC) is a malignant tumor of the thyroid gland. It is composed of C-cells and accounts for up to 2% of all thyroid cancers (1). Around 25% of MTCs arise due to germline mutations in the "rearranged during transfection" (*RET*) gene as part of Multiple Endocrine Neoplasia type 2 syndrome, while the remaining forms are sporadic. The genomic landscape of recurrent driver alterations found in sporadic disease seems to be mainly restricted to activating mutations affecting the *RET* (2) or *RAS* oncogenes (3, 4). There is a distinct genotype-phenotype correlation for each of these alterations (3, 5, 6). The RET^{M918T} mutation seems to trigger the most aggressive disease, showing poor prognosis with a higher prevalence of distant metastases during follow-up (5, 7). MTC cases with advanced disease are treated with tyrosine kinase inhibitors (TKIs), such as Vandetanib or Cabozantinib, which have shown to have therapeutic benefits. However, many patients suffer secondary toxicities that lead to dose reductions or treatment interruption (8, 9). A comprehensive understanding of the molecular mechanisms driving the different genetic classes of this disease is required to identify new therapeutic opportunities for these patients.

High-throughput technologies have already been used to define genomic signatures linked to particular driver mutations in cell lines and other thyroid cancer subtypes (10-15), uncovering molecular events associated with progression and recurrence. However, data on MTC are scarce due to the disease's low prevalence and, in consequence, the difficulty in collecting an informative sample set. On top of that, C-cells represent less than 1% of the thyroid gland, and therefore it is very challenging to portray their normal genomic landscape. To date, only a handful of studies using mRNA expression arrays have been published, reporting that MTC expression profiles are mutation-specific (16-18). Interestingly, the over-expression of genes related to the tumor growth factor beta pathway (17) and tumor invasion and metastases (16, 18) were notable among MTCs caused by the RET^{M918T} mutation. On the other hand, the miRNA profiling studies published so far have focused on patient outcomes rather

than on genetic subtypes of the disease, but have nevertheless uncovered some molecular events related to metastasis and worse outcomes (19-21).

Some of the differentially expressed genes identified in the previous profiling studies are undoubtedly regulated by aberrant methylation. However, explorations of this epigenetic mechanism in MTC, the deregulation of which is a well-known hallmark of cancer, have been limited, either focused on specific candidate genes, such as *RAS* association domain family protein 1 (*RASSF1*) (22) and Sprouty 1 (*SPRY1*) (23), or exploring the whole methylome in very few samples (15). Thus, it remains poorly characterized.

Therefore, we studied the role of aberrant DNA methylation in the pathology of genetic subtypes of MTC. We quantitatively profiled the largest cohort of medullary thyroid carcinomas published to date, composed of 48 samples, based on the DNA methylation levels of >27,000 CpGs across the genome. We observed significant differences between the methylation patterns among the samples carrying distinct mutations. Taking advantage of multilayer genomic data consisting of the transcriptome, miRNome and methylome, we uncovered genes negatively regulated by methylation. Moreover, pathway enrichment analysis underscored JAK/Stat pathway involvement in the RET^{M918T}-driven tumors. Using a series of 101 formalin-fixed paraffin-embedded (FFPE) MTC samples, we observed that phosphorylation of the JAK/Stat pathway effector STAT3 (Tyr705) was more evident among RET^{M918T}-positive tumors. *In vitro* pharmacological inhibition of STAT3 phosphorylation in two human MTC cell lines (MZ-CRC-1 and TT) revealed a higher dependency of the RET^{M918T}-mutated MZ-CRC-1 cell line on STAT3 signaling. Further, we observed an apparently synergistic effect between the action of STAT3 inhibitor and Vandetanib, which could be exploited to treat MTC patients.

MATERIALS AND METHODS

Human MTC tissue samples

Forty-eight fresh frozen MTC tumor samples were collected at the Spanish National Cancer Research Center (CNIO) in collaboration with the CNIO Tumor Bank. Written informed consent was obtained from all study participants and the study was approved by the relevant institutional review board (*Comité de bioética y bienestar animal* of the *Instituto de Salud Carlos III*). Sections of each sample were evaluated by a pathologist. Only samples in which at least 80% of cells were cancerous were used in this study, and cases with high amyloid content were excluded. A total of 101 paraffin-embedded (FFPE) MTC samples from unrelated individuals were used for validation studies. Twenty-five were used for the validation of DNA functional methylation markers, and the entire collection was used for an immunohistochemical study. Hematoxylin and eosin stained sections of each FFPE tumor sample were examined by a pathologist to select MTC areas representative of each tumor and these were used to construct tissue microarrays (TMA). Three TMAs containing 2 cores from each of 94 tumor samples were constructed. The remaining 7 tumors were evaluated as complete sections.

Cell lines and culture conditions

MZ-CRC-1 and TT cell lines were provided by Dr. James Fagin (Human Oncology & Pathogenesis Program, Memorial Sloan Kettering Cancer Centre, New York, USA) and authenticated by *RET* sequencing. The MZ-CRC-1 cell line is derived from a metastatic MTC and harbors the RET^{M918T} mutation, while TT cell line harbors a mutation in the 634th codon of *RET*. MZ-CRC-1 and TT were cultured in Dulbecco's modified Eagle medium GlutaMAX (DMEM, Invitrogen) and F12 Nut Mix medium with GlutaMAX (Invitrogen), respectively, supplemented with 10% (v/v) fetal bovine serum (FBS, PAA laboratories), 1% (v/v) penicillin/streptomycin and 0.6% (v/v) Fungizone (Gibco).

DNA, RNA and protein extraction

Genomic DNA from all samples (frozen and FFPE tumors and cell lines) was extracted using the DNeasy Blood and Tissue kit (Qiagen) according to the manufacturer's protocol. Total RNA was extracted from $5x10^6$ of MZ-CRC-1 and TT cells and 1 ml of TRIzol® (Life Technologies) using the standard conditions. For immunoblotting, cells lysates were produced in RIPA lysis buffer (Sigma) containing protease inhibitor mixture (Sigma) and Phosphatase Inhibitor Cocktail 2&3 (Sigma).

Mutation analysis

All samples were screened for hotspot mutations in exons 8, 10, 11, 13, 14, 15 and 16 of *RET* by Sanger sequencing. If negative, the hotspot codons 12, 13 and 61 of exons 2 and 3 of all *RAS* genes were screened using the same technique. Primer sequences and examples of the identified mutations can be found in Supplementary Table S1. Tumors were classified as "wild-type" (WT) if no mutation was found.

DNA methylation assay, data processing and data analysis

Genomic DNA was bisulfite-converted using the EZ DNA Methylation Kit (Zymo Research, Orange, CA) following the manufacturer's recommended procedures. Genome-wide promoter DNA methylation was determined using the Illumina Infinium HumanMethylation 27K Platform (Illumina, San Diego, CA, USA) as described previously (24). This assay generates DNA methylation data for 27,578 CpG dinucleotides covering 14,473 genes. For each CpG site, methylation levels were quantified using β-values, which represent the proportion of methylation, calculated as M/(M+U), where M is the methylated probe intensity and U the unmethylated probe intensity. β-values range from 0 to 1, with 0 being completely unmethylated and 1 being completely methylated. We excluded probes designed for sequences on either the X or the Y chromosome (1085 or 7 probes, respectively), as well as 46 probes with missing value in at least one sample. The data used in these analyses have been deposited in NCBI's Gene Expression Omnibus and are accessible through GEO Series accession number GSE72729

(http://www.ncbi.nlm.nih.gov/geo/query/acc.cgi?acc=GSE72729). The applied analysis workflow is schematically depicted in Supplementary Figure S1.

Unsupervised hierarchical clustering was carried out using Cluster 3.0 software with "average linkage" (Pearson correlation, uncentered metrics). The clusters were subsequently visualized using Treeview (http://rana.stanford.edu/software). Principal component analysis (PCA) was performed using R CRAN version 2.15.3 (R, 2013). Differences in DNA methylation status among tumor groups (based on the driver mutations present in the samples) were tested using POMELO II, applying linear models (limma) (25). Only groups containing at least 5 tumors were considered. Each genetic class was compared to WT tumors, and with each of the other classes. To account for multiple hypothesis testing, *p*-values were adjusted using Benjamini and Hochberg's false discovery rate (FDR) correction. We defined a probe to be hypomethylated or hypermethylated when it displayed a mean β-value difference (Δβ-value) < -0.2 or > 0.2, respectively, calculated as mean difference among distinct tumor groups, and had a FDR<0.05. With the extracted lists of differentially methylated genes, we performed Venn diagram analyses using BioVenn (http://www.cmbi.ru.nl/cdd/biovenn/) and Pathway enrichment analysis using the functional annotation clustering tool implemented in DAVID Bioinformatics Resources 6.7 (http://david.abcc.ncifcrf.gov/home.jsp).

Since we had both mRNA (18) and miRNA expression (GEO Series accession number GSE72728 [http://www.ncbi.nlm.nih.gov/geo/query/acc.cgi?acc=GSE72728]) data for 33 and 31 of the tumors used in this study, respectively, we aimed to identify genes whose expression is correlated with the methylation status of their corresponding promoter regions. Expression of all the available protein-coding genes identified as differentially methylated by tumor genotype (FDR < 0.05, |Δβ –value| > 0.2) was examined as previously described (12, 26). The integration of miRNA data required a genome-wide approach since there was only one microRNA gene promoter showing differential methylation. More specifically, there were 254 probes included on the methylation platform that mapped to promoters of 110 microRNA genes previously annotated by the manufacturer (24). To this number, we added 423 probes belonging to putative

promoter regions of 151 miRNAs identified using the PROmiRNA method (27). These additional probes and their corresponding miRNA genes are listed in Supplementary Table S2. Correlation was measured by the Spearman coefficient using R CRAN version 2.15.3 (R, 2013) and genes with a negative correlation coefficient and p-value<0.05 were considered significantly correlated.

Confirmation of inverse correlation between methylation and expression in MTC cell lines

To confirm the effect of DNA methylation on gene expression, MZ-CRC-1 cells at 60% of confluence were treated with 50 µg/ml 5-Aza-2-'Deoxycytidine (Sigma). This treatment was repeated every 48 hours over 6 days and then the cells were collected for RNA and DNA extraction.

DNA methylation level assessment

Bisulfite sequencing of MTC cell lines using the primers listed in Supplementary Table S3 was carried out according to protocols described elsewhere (12) in order to assess methylation level of the selected promoters (belonging to 3 protein-coding genes and 3 miRNA genes).

qRT-PCR

For the assessment of expression of the selected protein-coding genes, one microgram of total RNA was reverse transcribed using Superscript II (Invitrogen) and an oligo dT_{14} primer following manufacturer's instructions. The amounts of *DKK4*, *MMP20* and *PLCB2* mRNA were quantified by real-time PCR with QuantStudio 6 Flex Real-Time PCR system (Applied Biosystems), using primers designed to be specific for the three genes (Supplementary Table S3) and probes from the Universal ProbeLibrary Set, Human (Roche). Normalization was carried out with the internal standard β-actin (*ACTB*).

For miRNA gene expression quantification, 10 nanograms of total RNA were used for first-strand cDNA synthesis using the miRCURY LNA Universal RT miR PCR system

(Exiqon) and LNA miR-PCR primer/SYBR Green mix (Exiqon) was used for subsequent quantification of miR-10a, -30a and -200c according to the manufacturer's recommendations. MiR-16 was selected as the reference gene for normalization.

Negative controls were included in all PCR series and assays were carried out in triplicate. The $\Delta\Delta C$t method was used for the calculation of mRNA/miRNA content (28).

Methylation status validation

Three of the most differentially methylated probes, all showing negative correlation with expression of the corresponding protein-coding gene, and with biological functions potentially relevant to MTC were selected for validation. The technical validation of microarray results in a subset of the original discovery series (comprising 6 *RET*^{M918T}, 6 *RET*^{C634}, 3 *RAS*, 2 "wild-type" tumors and 6 tumors bearing other *RET* mutations) was performed using bisulfite sequencing, as described elsewhere (12). The candidate functional methylation markers were then validated by pyrosequencing in 25 independent FFPE MTC samples (8 *RET*^{M918T}, 4 *RET*^{C634}, 3 *RAS* and 10 "wild-type" tumors). The region of interest, including the CpG assessed by the Infinium array, was first amplified from the bisulfite-treated DNA by a set of primers designed using the PyroMark assay design software (version 2.0.01.15). Following PCR amplification, pyrosequencing was performed using PyroMark Q24 reagents, vacuum prep workstation, equipment and software (Qiagen). The primers used in these steps are listed in Supplementary Table S3.

Immunohistochemical study

Three paraffin-embedded TMAs and 7 complete sections were used for the evaluation of a JAK/Stat pathway effector pSTAT3 (Tyr705). Monoclonal antibody was obtained from Cell Signaling Technology (#9145). Two independent experienced pathologists (X.M.-G. and M.S.) evaluated the staining by visual examination under a microscope. Since each TMA included two different tumor cores from each case, immunohistochemical scoring was done after examining both samples. When the two cores gave inconsistent results, the complete

section of the corresponding tumor was evaluated. Samples were scored from 0 (no immunostaining) to 300 (intensive immunostaining) depending on both the intensity and extension of staining.

Inhibitor treatment and cell proliferation assay

For the study of proliferation inhibition by TKI and the inhibition of the phosphorylation of STAT3, Vandetanib (Seleckchem) and LLL12 (EMD Millipore) (29) were made up as a stock solution of 5 mM in dimethylsulfoxide (DMSO). MZ-CRC-1 and TT cells were plated in 200 µl of medium at concentrations of $2x10^4$ cells per well. After 36 hours, cells were treated with increasing concentrations of the indicated compounds (0; 0.005; 0.05; 0.1; 0. 5; 1; 2.5; 5 µM). A concentration of 0.1% DMSO was used in all conditions. This treatment was repeated every 4 days. Proliferation was measured at 10 days using a cell proliferation kit (WST-1 reagent, Roche). The concentration that led to 50% growth inhibition (IC_{50}) was calculated using GraphPad Prim. All experiments were performed in triplicate. For the combinational treatment we also used the above-mentioned experimental scheme. A fixed concentration of 0.04 µM of LLL12 was combined with increasing concentrations of Vandetanib (0; 0.005; 0.05; 0.1; 0. 5; 1; 2.5; 5 µM). The suboptimal LLL12 concentration (0.04 µM) used causes only 10% growth inhibition of MZ-CRC-1 cells. Additionally, for Western blot analysis, MZ-CRC-1 were treated with increasing concentrations of Vandetanib (0.01; 0.1; 0.5 µM), 0.04 µM LLL12 and a combination of LLL12 and Vandetanib (0.04 µM and 0.1 µM, respectively) for 24 hours. Cells were then washed with ice-cold PBS, collected by scraping, and cell lysates were prepared using the above-mentioned protocol. The following primary antibodies were used for immunoblotting: p-ERK, pAKT, pSTAT3 and GAPDH (Cell Signaling; #9101, #4060, #9145 and #2118, respectively). Absolute band intensities of the indicated proteins were captured and quantified with the Image Lab software v4.1 (BioRad). GAPDH was used as loading control normalizer. Data were expressed in relative units using the control condition as reference.

RESULTS

Molecular characterization of the MTC discovery series

Among the tumors whose genome-wide DNA methylation levels were measured, 36 (75%) harbored a *RET* mutation (13 carried the RET^{M918T} mutation, 14 RET^{C634} and 9 less frequent *RET* mutations), and 6 (12.5%) tumors harbored a *RAS* mutation. The remaining 6 tumors (12.5%) did not carry any alteration in the studied genes and were considered "wild-type" (WT). The results of the mutational screening together with the main clinico-histopathological characteristics of the samples are summarized in the Supplementary Table S4.

MTC methylation profiles relate closely to *RET* mutational status

We identified 11,915 probes that were constitutively unmethylated (β-value <0.2) in all samples. According to DAVID functional enrichment analysis (30), the majority (97.5%) of these were located within CpG islands adjacent to house-keeping genes (Benjamini-Hochberg adjusted *p*-value = 7.1×10^{-10}). On the other hand, 179 probes were constitutively methylated (β-values>0.8 for all samples). Both constitutively unmethylated and methylated probes were excluded from further analyses. A PCA of the remaining 14,346 probes (belonging to 9,216 consensus coding sequences) did not identify any batch effects affecting the data (Supplementary Figure S2).

Unsupervised hierarchical analysis using the 851 probes with the variance >0.2 identified two principal clusters that differed in their underlying genetics (Figure 1). Only two samples did not fall into either cluster. Interestingly, cluster B showed higher levels of methylation when compared to cluster A (*p*-value = 3.0×10^{-9}), and was enriched with WT cases and those harboring the RET^{C634} mutation, while cluster A was composed mostly of RET^{M918T}-positive tumors (p-value<0.02). We did not observe any clear clustering of the *RAS*-mutated samples.

Supervised analysis according to driver mutation allowed us to identify a list of differentially methylated probes associated with specific mutations, which was especially long

for *RET*^{M918T}-related tumors. These findings confirmed those from the unsupervised clustering, since in this group there were more hypomethylated probes (Figure 2A&2B, Supplementary Table S5). The protein-coding gene *DKK4* (Dickkopf WNT Signaling Pathway Inhibitor 4), previously described to be up-regulated in *RET*^{M918T}-related MTCs (18), was one of the genes affected by hypomethylation among *RET*^{M918T}-positive carcinomas. Also consistent with the unsupervised clustering result, the lists of differentially methylated probes characteristic of the other genetic conditions (*RET*^{C634}- and *RAS*-related tumors) when comparing to WT, were considerably shorter (Figure 2B). Nevertheless, hypomethylation of *GAL* was detected among *RET*^{C634}-positive tumors when comparing to WT, and this event could cause the increased expression of this molecule reported elsewhere (18).

Hypermethylation more frequently affected probes located within CpG islands (p-value 0.0014) as well as those located near stem cell PolyComb Group target genes (p-value<0.0001). Hypomethylated probes, on the other hand, were enriched with CpGs that are heavily methylated in embryonic stem cells (p-value<0.0001) (Figure 2C).

OMIC data integration reveals potentially functional DNA methylation changes in MTC

The above findings indicated that some epigenetic changes can have a functional consequence, which encouraged us to systematically explore genes (protein- and miRNA-coding) regulated by methylation at their promoters (see Supplementary Figure S1 for further details). mRNA expression data was available for > 91% of protein coding genes that were differentially methylated based on tumor genotype. A negative correlation between expression and methylation was observed for 5% of these (Supplementary Figure S3). *PLCB2*, *DKK4*, *MMP20* were selected for further study since they have been previously described to have a role in the promoting tumor growth (18, 31-33). Moreover, a genome-wide assessment of methylation and miRNA expression of matching samples identified 5 miRNA genes (6.9%) showing negative correlation (Supplementary Figure S3). MiR-10a was also found as differentially methylated in the previous supervised analyses and was selected for further

studies. Two additional miRNA genes (miR-30a and -200c) showing negative correlation between expression and methylation, and a tendency towards differential methylation (FDR<0.15) in supervised clustering, were also studied further due to their biological function (21, 34, 35). As assessed by bisulfite sequencing, the levels of methylation of the 6 genes (3 protein-coding and 3 microRNAs) differed between the two available MTC cell lines (Figure 3A). Apart from two genes that were not expressed by either of the cell lines (*MMP20* and miR-30a), the expression of the other four genes confirmed the results of *in silico* predictions of inverse correlation between DNA methylation and gene expression (Figure 3B). Since MZ-CRC-1 showed systematically higher levels of DNA methylation of these six loci, we treated it with the demethylating agent 5-Aza-2-'Deoxycytidine. A higher expression of all genes in the MZ-CRC-1 cell line was detected in the treated condition as compared to untreated one (Figure 3C), further confirming the functional effect of these epigenetic changes.

Validation of aberrant methylation of candidate oncogenes

CpGs from the promoters of 3 differentially methylated genes (*DKK4*, *MMP20*, *PLCB2*) were selected for validation. These genes also showed a negative correlation between DNA methylation levels and gene expression (Supplementary Figure S3). As depicted in Figure 4, the results of bisulfite sequencing in a subset of the original series revealed a high correlation with the array-based measures (R^2 ranging from 0.66 to 0.80). Moreover, we were able to replicate the findings by bisulfite pyrosequencing of an independent series of 25 FFPE MTCs (Figure 4), although the difference between the DNA methylation levels of the compared groups was smaller, probably because the DNA source was paraffin tissue.

Multi-OMIC data and pathway enrichment analyses uncover JAK/Stat pathway involvement in *RET*^{M918T} MTCs

Functional annotation clustering by DAVID (30) of the genes with aberrant methylation (Supplementary Figure S4) and by GSEA of differentially expressed genes (18) among *RET*^{M918T}-positive carcinomas uncovered a significant enrichment for signaling pathways such

as cytokine-cytokine receptor interaction (p-value=$1.5x10^{-7}$) and JAK/Stat (p-value=$2.3x10^{-4}$). STAT3 is a JAK/Stat pathway effector and a putative downstream target of RET (36). Thus, we assessed by immunohistochemistry its active phosphorylated form (at Tyr705) in 101 MTC samples. *RET*^{M918T}-related tumors were more frequently and intensively positively stained than the other genetic classes (p-value<0.02, Figure 5A) confirming activation of the JAK/Stat cascade and the *in silico* prediction. We aimed to exploit these differences to study *in vitro* the functional relevance of STAT3 activation in MTC. As revealed by proliferation assay, MZ-CRC-1 cells were more sensitive to inhibition of STAT3 phosphorylation than TT cells (IC_{50}(MZ-CRC-1) = 0.06 μM, IC_{50}(TT) = 0.23 μM, Figure 5B). In fact, the *RET*^{M918T}-mutated cell line showed a higher sensitivity to this treatment than to the standard of care, TKI Vandetanib (IC_{50}(MZ-CRC-1) = 0.62 μM, Figure 5B).

Since STAT3 is a downstream point of convergence for many growth factor pathways, synergy may be expected when combined with other inhibitors (37). A suboptimal dose of pSTAT3 inhibitor, when combined with Vandetanib, apparently showed a synergistic effect on cell growth inhibition of *RET*^{M918T}-positive cells (Figure 5C). Moreover, treatment with Vandetanib produced a dose-dependent inhibition of pSTAT3 in MZ-CRC-1, and suboptimal combinational treatment of the two drugs (0.04 μM LLL12 with 0.1 μM Vandetanib) potentiated the inhibitory effect on both canonical (pERK, pAKT) and non-canonical (pSTAT3) effectors of RET downstream signaling (Figure 5D).

DISCUSSION

The current genomic era offers great opportunities to answer many clinically relevant questions concerning various types of cancer through comprehensive and integrative analyses of OMIC data. Some cancer types are being neglected by these efforts, generally due to their low prevalence, and thus small overall public health impact. Medullary thyroid carcinoma is one of the least prevalent subtypes of thyroid cancer, but is responsible for a large proportion of thyroid cancer-related deaths (38), mainly because treatment with cytotoxic drugs and/or standard radiotherapy has been proven to be ineffective (39).

Using the largest cohort of MTC samples reported to date, we have applied a multilayer OMIC data integration focused on the effects of DNA methylation in the etiology of this tumor. The current work is the first to report not only that underlying genetics relates closely to genome-wide DNA methylation fingerprints, but also that the aberrant methylation events affect specific genomic loci (for example, PolyComb targets) pointing to the existence of an epigenetic progenitor cell signature in MTC (40). Furthermore, we identify both protein-coding and microRNA genes, the expression of which is negatively correlated with the methylation status of their promoters, and we confirm some of these findings in MTC cell lines. We propose promoter methylation of *MMP20*, *DKK4* and *PLCB2* as functional epigenetic markers of MTC genetic classes. The integrative approach allowed us to uncover the involvement of the JAK/Stat pathway in RET^{M918T}-related MTCs, which apparently sustains the proliferative features of the MTC cell model for this genetic class.

DNA methylation is traditionally believed to be a regulator of gene expression. In the case of protein-coding genes, the classical view of the negative effect of methylation on expression is being challenged by recent technical advances. Many cancer-orientated studies, including the current one, report a surprisingly low percentage of genes for which this inverse relationship applies (26). The situation with microRNAs is even more complex, given the difficulties with identifying their promoter regions (41). Recently, a methodology became

available that recognizes putative promoter regions of miRNAs using both sequence- and histone-based techniques (27). By integrating this strategy in our analysis, we were able to identify CpGs belonging to additional putative miRNA promoters included on the 27K array. The overall portion of miRNA genes for which a negative correlation between methylation and expression was observed was similar to that for protein-coding genes. Nevertheless, for the majority of the genes selected for validation of the inverse correlation between expression and methylation in MTC cell lines, we were able to functionally confirm the *in silico* predictions. One of these genes, *DKK4*, has previously been linked to MTC pathogenesis (18), and here we propose aberrant methylation as the regulatory mechanism responsible for its over-expression in *RET*^{M918T}-related tumors. On the other hand, *PLCB2* plays a role in multiple transmembrane signal transduction pathways involving inositol lipid metabolism. In cancer, its over-expression has been associated with mitosis promotion, migration and poor outcome (31, 42). Our finding of hypomethylation in the *RET*^{M918T}-positive tumor samples, which was negatively associated with increased *PLCB2* expression, is consistent with this gene having a cancer-promoting role. Even though the prognostic utility of *MMP20,* a member of the family of metalloproteinases, has already been demonstrated in cancer (32), we did not detect its expression in the studied cell lines. Nevertheless, its validation in an independent series of MTC carcinomas confirms its potential utility as a methylation marker of *RET*^{M918T}-related tumors.

Regarding miRNA genes, the expression of miR-200c has been recently described as causative of the metastatic potential of human MTCs (21). Interestingly, according to our results in MTC cell lines, the aberrant methylation of the putative promoter of miR-200c could underlie its differential expression among patients with distinct disease outcomes. MiR-10a mostly exerts an oncogenic effect (43, 44) and we found little DNA methylation of its promoter in both MTC cell lines. There is evidence from hepatocellular carcinoma that miR-10a is negatively regulated by DNA methylation (45), which was further validated by our findings. MiR-30a warrants further study due to its tumor-suppressive features (34, 35). PROM1, a cancer stem cell marker found over-expressed in *RET*^{M918T}-positive tumors (18), is one of its predicted

targets, according to targetscan tool (http://www.targetscan.org/). Our findings indicate that a hypermethylation-driven down-regulation of miR-30a could lead to an up-regulation of its target PROM1.

Our integrated analysis pointed to the involvement of signaling networks such as cytokine-cytokine interaction and JAK/Stat in *RET*^{M918T} tumors. These pathways have previously been related to malignant tumor behavior, which is consistent with the observation that these MTC patients have the worst clinical outcomes (5). The genetic class-specific implication of JAK/Stat pathways was confirmed by IHC in a large number of human tumors. This is in line with previous *in vitro* findings from 293T cells transfected with wild-type RET or RET^{M918T}, where only the latter induced constitutive phosphorylation of STAT3. On top of that, RET^{M918T} was far more efficient in recruiting STAT3 protein than both RET^{C634} and wild-type RET *in vitro* (46). Constitutive activation of STAT3 has been reported at high frequency in large numbers of malignant cell lines, *in vivo* animal models and human tumors (reviewed in (37)). In general, activation of STAT3 is associated with a worse prognosis due to its role in uncontrollable proliferation and modulation of microenvironment (reviewed in (47)). Thus, STAT3 is a very attractive molecule for targeted therapies (reviewed in (48)). Indeed, while no drug has shown promising results in clinical trials (49), it has been suggested that inhibition of STAT3 signaling in combination with other therapies (targeted therapies or radiotherapy) could lead to clinical benefit (50). We found that low doses of the inhibitor of pSTAT3 increased the sensitivity of MTC cells to Vandetanib treatment. This could have an important impact on the management of MTC patients, since Vandetanib treatment leads to frequent toxicities, which require dose reductions or even discontinuation (8).

In summary, this comprehensive integrative genomic study performed using the largest cohort of MTC samples reported to date, provides insights into the involvement of DNA methylation in the etiology of this disease. We confirmed the regulatory role of DNA methylation for *DKK4, PLCB2, MMP20,* miR-10a, miR-30a and miR-200c using MZ-CRC-1 and TT cell lines. Moreover, hypomethylation may induce activation of key pathways related to

the malignant behavior of *RET*^{M918T}-related MTCs. Inhibition of one of these – the STAT3 signaling pathway – sensitizes *RET*^{M918T}-mutated MTC cells to standard Vandetanib treatment.

ACKNOWLEDGMENTS

We thank Manuel Morente and María Jesús Artiga from the Spanish National Tumor Bank Network (CNIO) for their hard work collecting the tumor samples used in this study. We also thank Magdolna Djurec and Teresa Blasco for their help with the western blot analysis.

REFERENCES

1. DeLellis RA, Lloyd RV, Heitz PU,Eng C, World Health Organization Classification of Tumours. Tumours of Endocrine Organs. **2004**, Lyon: IARC Press.
2. Leboulleux S, Baudin E, Travagli JP,Schlumberger M. Medullary thyroid carcinoma. *Clin Endocrinol (Oxf).* **2004**;61(3): 299-310.
3. Ciampi R, Mian C, Fugazzola L, Cosci B, Romei C, Barollo S*, et al.* Evidence of a low prevalence of RAS mutations in a large medullary thyroid cancer series. *Thyroid.* **2013**;23(1): 50-7.
4. Moura MM, Cavaco BM, Pinto AE,Leite V. High prevalence of RAS mutations in RET-negative sporadic medullary thyroid carcinomas. *J Clin Endocrinol Metab.* **2011**;96(5): E863-8.
5. Elisei R, Cosci B, Romei C, Bottici V, Renzini G, Molinaro E*, et al.* Prognostic significance of somatic RET oncogene mutations in sporadic medullary thyroid cancer: a 10-year follow-up study. *J Clin Endocrinol Metab.* **2008**;93(3): 682-7.
6. Romei C, Elisei R, Pinchera A, Ceccherini I, Molinaro E, Mancusi F*, et al.* Somatic mutations of the ret protooncogene in sporadic medullary thyroid carcinoma are not restricted to exon 16 and are associated with tumor recurrence. *J Clin Endocrinol Metab.* **1996**;81(4): 1619-22.
7. Schilling T, Burck J, Sinn HP, Clemens A, Otto HF, Hoppner W*, et al.* Prognostic value of codon 918 (ATG-->ACG) RET proto-oncogene mutations in sporadic medullary thyroid carcinoma. *Int J Cancer.* **2001**;95(1): 62-6.
8. Durante C, Paciaroni A, Plasmati K, Trulli F,Filetti S. Vandetanib: opening a new treatment practice in advanced medullary thyroid carcinoma. *Endocrine.* **2013**.
9. Kurzrock R, Sherman SI, Ball DW, Forastiere AA, Cohen RB, Mehra R*, et al.* Activity of XL184 (Cabozantinib), an oral tyrosine kinase inhibitor, in patients with medullary thyroid cancer. *J Clin Oncol.* **2011**;29(19): 2660-6.
10. Giordano TJ, Kuick R, Thomas DG, Misek DE, Vinco M, Sanders D*, et al.* Molecular classification of papillary thyroid carcinoma: distinct BRAF, RAS, and RET/PTC mutation-specific gene expression profiles discovered by DNA microarray analysis. *Oncogene.* **2005**;24(44): 6646-56.
11. Hou P, Liu D,Xing M. Genome-wide alterations in gene methylation by the BRAF V600E mutation in papillary thyroid cancer cells. *Endocr Relat Cancer.* **2011**;18(6): 687-97.
12. Mancikova V, Buj R, Castelblanco E, Inglada-Perez L, Diez A, de Cubas AA*, et al.* DNA methylation profiling of well-differentiated thyroid cancer uncovers markers of recurrence free survival. *Int J Cancer.* **2014**.
13. Mancikova V, Castelblanco E, Pineiro-Yanez E, Perales-Paton J, de Cubas AA, Inglada-Perez L*, et al.* MicroRNA deep-sequencing reveals master regulators of follicular and papillary thyroid tumors. *Mod Pathol.* **2015**.
14. Montero-Conde C, Martin-Campos JM, Lerma E, Gimenez G, Martinez-Guitarte JL, Combalia N*, et al.* Molecular profiling related to poor prognosis in thyroid carcinoma. Combining gene expression data and biological information. *Oncogene.* **2008**;27(11): 1554-61.
15. Rodriguez-Rodero S, Fernandez AF, Fernandez-Morera JL, Castro-Santos P, Bayon GF, Ferrero C*, et al.* DNA methylation signatures identify biologically distinct thyroid cancer subtypes. *J Clin Endocrinol Metab.* **2013**;98(7): 2811-21.
16. Ameur N, Lacroix L, Roucan S, Roux V, Broutin S, Talbot M*, et al.* Aggressive inherited and sporadic medullary thyroid carcinomas display similar oncogenic pathways. *Endocr Relat Cancer.* **2009**;16(4): 1261-72.
17. Jain S, Watson MA, DeBenedetti MK, Hiraki Y, Moley JF,Milbrandt J. Expression profiles provide insights into early malignant potential and skeletal abnormalities in multiple endocrine neoplasia type 2B syndrome tumors. *Cancer Res.* **2004**;64(11): 3907-13.

18. Maliszewska A, Leandro-Garcia LJ, Castelblanco E, Macia A, de Cubas A, Gomez-Lopez G, *et al.* Differential gene expression of medullary thyroid carcinoma reveals specific markers associated with genetic conditions. *Am J Pathol.* **2013**;182(2): 350-62.
19. Abraham D, Jackson N, Gundara JS, Zhao J, Gill AJ, Delbridge L, *et al.* MicroRNA profiling of sporadic and hereditary medullary thyroid cancer identifies predictors of nodal metastasis, prognosis, and potential therapeutic targets. *Clin Cancer Res.* **2011**;17(14): 4772-81.
20. Nikiforova MN, Tseng GC, Steward D, Diorio D,Nikiforov YE. MicroRNA expression profiling of thyroid tumors: biological significance and diagnostic utility. *J Clin Endocrinol Metab.* **2008**;93(5): 1600-8.
21. Santarpia L, Calin GA, Adam L, Ye L, Fusco A, Giunti S, *et al.* A miRNA signature associated with human metastatic medullary thyroid carcinoma. *Endocr Relat Cancer.* **2013**;20(6): 809-23.
22. Schagdarsurengin U, Gimm O, Hoang-Vu C, Dralle H, Pfeifer GP,Dammann R. Frequent epigenetic silencing of the CpG island promoter of RASSF1A in thyroid carcinoma. *Cancer Res.* **2002**;62(13): 3698-701.
23. Macia A, Gallel P, Vaquero M, Gou-Fabregas M, Santacana M, Maliszewska A, *et al.* Sprouty1 is a candidate tumor-suppressor gene in medullary thyroid carcinoma. *Oncogene.* **2012**;31(35): 3961-72.
24. Bibikova M, Le J, Barnes B, Saedinia-Melnyk S, Zhou L, Shen R, *et al.* Genome-wide DNA methylation profiling using Infinium(R) assay. *Epigenomics.* **2009**;1(1): 177-200.
25. Morrissey ER,Diaz-Uriarte R. Pomelo II: finding differentially expressed genes. *Nucleic Acids Res.* **2009**;37(Web Server issue): W581-6.
26. Selamat SA, Chung BS, Girard L, Zhang W, Zhang Y, Campan M, *et al.* Genome-scale analysis of DNA methylation in lung adenocarcinoma and integration with mRNA expression. *Genome Res.* **2012**;22(7): 1197-211.
27. Marsico A, Huska MR, Lasserre J, Hu H, Vucicevic D, Musahl A, *et al.* PROmiRNA: a new miRNA promoter recognition method uncovers the complex regulation of intronic miRNAs. *Genome Biol.* **2013**;14(8): R84.
28. Livak KJ,Schmittgen TD. Analysis of relative gene expression data using real-time quantitative PCR and the 2(-Delta Delta C(T)) Method. *Methods.* **2001**;25(4): 402-8.
29. Lin L, Hutzen B, Li PK, Ball S, Zuo M, DeAngelis S, *et al.* A novel small molecule, LLL12, inhibits STAT3 phosphorylation and activities and exhibits potent growth-suppressive activity in human cancer cells. *Neoplasia.* **2010**;12(1): 39-50.
30. Huang da W, Sherman BT,Lempicki RA. Systematic and integrative analysis of large gene lists using DAVID bioinformatics resources. *Nat Protoc.* **2009**;4(1): 44-57.
31. Bertagnolo V, Benedusi M, Brugnoli F, Lanuti P, Marchisio M, Querzoli P, *et al.* Phospholipase C-beta 2 promotes mitosis and migration of human breast cancer-derived cells. *Carcinogenesis.* **2007**;28(8): 1638-45.
32. Liu Y, Li Y, Liu Z, Zhang L, Anniko M,Duan M. Prognostic significance of matrix metalloproteinase-20 overexpression in laryngeal squamous cell carcinoma. *Acta Otolaryngol.* **2011**;131(7): 769-73.
33. Takeuchi S, Wada K, Toyooka T, Shinomiya N, Shimazaki H, Nakanishi K, *et al.* Increased xCT expression correlates with tumor invasion and outcome in patients with glioblastomas. *Neurosurgery.* **2013**;72(1): 33-41; discussion
34. Cheng CW, Wang HW, Chang CW, Chu HW, Chen CY, Yu JC, *et al.* MicroRNA-30a inhibits cell migration and invasion by downregulating vimentin expression and is a potential prognostic marker in breast cancer. *Breast Cancer Res Treat.* **2012**;134(3): 1081-93.
35. Kumarswamy R, Mudduluru G, Ceppi P, Muppala S, Kozlowski M, Niklinski J, *et al.* MicroRNA-30a inhibits epithelial-to-mesenchymal transition by targeting Snai1 and is downregulated in non-small cell lung cancer. *Int J Cancer.* **2012**;130(9): 2044-53.
36. de Groot JW, Links TP, Plukker JT, Lips CJ,Hofstra RM. RET as a diagnostic and therapeutic target in sporadic and hereditary endocrine tumors. *Endocr Rev.* **2006**;27(5): 535-60.

37. Wang X, Crowe PJ, Goldstein D,Yang JL. STAT3 inhibition, a novel approach to enhancing targeted therapy in human cancers (review). *Int J Oncol.* **2012**;41(4): 1181-91.
38. Roman S, Lin R,Sosa JA. Prognosis of medullary thyroid carcinoma: demographic, clinical, and pathologic predictors of survival in 1252 cases. *Cancer.* **2006**;107(9): 2134-42.
39. Orlandi F, Caraci P, Mussa A, Saggiorato E, Pancani G,Angeli A. Treatment of medullary thyroid carcinoma: an update. *Endocr Relat Cancer.* **2001**;8(2): 135-47.
40. Zhuang J, Jones A, Lee SH, Ng E, Fiegl H, Zikan M*, et al.* The dynamics and prognostic potential of DNA methylation changes at stem cell gene loci in women's cancer. *PLoS Genet.* **2012**;8(2): e1002517.
41. Krol J, Loedige I,Filipowicz W. The widespread regulation of microRNA biogenesis, function and decay. *Nat Rev Genet.* **2010**;11(9): 597-610.
42. Bertagnolo V, Benedusi M, Querzoli P, Pedriali M, Magri E, Brugnoli F*, et al.* PLC-beta2 is highly expressed in breast cancer and is associated with a poor outcome: a study on tissue microarrays. *Int J Oncol.* **2006**;28(4): 863-72.
43. Bryant A, Palma CA, Jayaswal V, Yang YW, Lutherborrow M,Ma DD. miR-10a is aberrantly overexpressed in Nucleophosmin1 mutated acute myeloid leukaemia and its suppression induces cell death. *Mol Cancer.* **2012**;11: 8.
44. Long MJ, Wu FX, Li P, Liu M, Li X,Tang H. MicroRNA-10a targets CHL1 and promotes cell growth, migration and invasion in human cervical cancer cells. *Cancer Lett.* **2012**;324(2): 186-96.
45. Shen J, Wang S, Zhang YJ, Kappil MA, Chen Wu H, Kibriya MG*, et al.* Genome-wide aberrant DNA methylation of microRNA host genes in hepatocellular carcinoma. *Epigenetics.* **2012**;7(11): 1230-7.
46. Yuan ZL, Guan YJ, Wang L, Wei W, Kane AB,Chin YE. Central role of the threonine residue within the p+1 loop of receptor tyrosine kinase in STAT3 constitutive phosphorylation in metastatic cancer cells. *Mol Cell Biol.* **2004**;24(21): 9390-400.
47. Thomas SJ, Snowden JA, Zeidler MP,Danson SJ. The role of JAK/STAT signalling in the pathogenesis, prognosis and treatment of solid tumours. *Br J Cancer.* **2015**;113(3): 365-71.
48. Debnath B, Xu S,Neamati N. Small molecule inhibitors of signal transducer and activator of transcription 3 (Stat3) protein. *J Med Chem.* **2012**;55(15): 6645-68.
49. Bendell JC, Hong DS, Burris HA, 3rd, Naing A, Jones SF, Falchook G*, et al.* Phase 1, open-label, dose-escalation, and pharmacokinetic study of STAT3 inhibitor OPB-31121 in subjects with advanced solid tumors. *Cancer Chemother Pharmacol.* **2014**;74(1): 125-30.
50. Lo HW, Cao X, Zhu H,Ali-Osman F. Constitutively activated STAT3 frequently coexpresses with epidermal growth factor receptor in high-grade gliomas and targeting STAT3 sensitizes them to Iressa and alkylators. *Clin Cancer Res.* **2008**;14(19): 6042-54.

TABLE AND FIGURE LEGENDS

Figure 1. Methylome of the discovery series. Unsupervised hierarchical cluster analysis of 48 medullary tumors divided the sample set into 2 main clusters. "Cluster A" was composed mostly of *RET*^{M918T}-related samples. "Cluster B" included the majority of *RET*^{C634}- and wild-type cases. Color codes used are as follows: red = *RET*^{M918T} mutation, black = *RET*^{C634} mutation, yellow = *RAS* mutation, transparent = other *RET* mutation, green = wild type.

Figure 2. Identification of differentially methylated probes. A) Volcano plots, from each of the supervised analysis carried out, identifying differentially hypomethylated (green) and hypermethylated (red) probes, defined based on FDR<0.05 and $|\Delta\beta\text{-value}| \geq 0.2$. **B)** Venn diagram showing the overlap between the identified mutation-specific hyper- and hypo-methylated probes from comparisons with WT tumors. **C)** Number of probes hypermethylated and hypomethylated, by location with respect to: CpG islands; gene targeted by PolyComb Repressive Complex; loci that are heavily methylated in embryonic stem cells.

Figure 3. Confirmation of negative correlation between methylation and gene expression in MZ-CRC-1 and TT cell lines. A) DNA methylation levels of promoter CpGs of *DKK4*, *PLCB2*, *MMP20*, miR-10a, -200c and -30a as measured by bisulfite sequencing. **B)** Expression of *DKK4*, *PLCB2*, *MMP20*, miR-10a, -200c and -30a shows an opposite trend as compared to the DNA methylation levels of the genes, confirming *in silico* results. **C)** 5-aza-2′-deoxycytidine (5AdC) treatment causes the reactivation of *DKK4*, *PLCB2*, *MMP20,* miR-10a, -200c and -30a expression in the MZ-CRC-1 cell line.

Figure 4 Validation of selected loci. Three CpGs from promoter regions of *MMP20*, *PLCB2* and *DKK4* were selected for validation. In the left panel, results from the discovery series are represented. In the middle panel, correlation between the results from Illumina Infinium HumanMethylation 27K Platform and bisulfite sequencing for selected loci is shown. Bisulfite sequencing was performed in a subset of samples included in the discovery series (6 *RET*^{M918T}, 6 *RET*^{C634}, 3 *RAS*, 2 "wild-type" tumors and 6 tumors bearing other *RET* mutations). In the right

panel, results of bisulfite pyrosequencing of 25 independent MTC samples (8 *RET*^{M918T}, 4 *RET*^{C634}, 3 *RAS* and 10 "wild-type" tumors) are depicted.

Figure 5. STAT3 signaling in *RET*^{M918T}-related MTC. A) Immunohistochemical study of 101 MTC samples. Staining was scored according to both extent and intensity. Each point represents one tumor staining result; bars represent the median value in a given genetic class. The most intense positive staining was detected among *RET*^{M918T}-positive MTCs (p-value=0.014). **B)** Effects of TKI and inhibitor of phosphorylation of STAT3 on MTC cell proliferation. MZ-CRC-1 and TT cell lines were treated with increasing concentrations of Vandetanib (Tyrosine Kinase Inhibitor) or LLL12 (Inhibitor of phosphorylation of STAT3) for 10 days. At day 10 the proliferation was assessed using WST-1 reagent. Average values of triplicated experiments are presented with error bars representing the standard deviation (SD). Concentration (listed in μM) leading to 50% of growth inhibition (IC_{50}) and the 95% confidence interval (95% CI) were determined using GraphPad Prim. **C)** LLL12 sensitized MZ-CRC-1 cells to Vandetanib treatment. MZ-CRC-1 cells were treated with a fixed sub-IC_{50} concentration of LLL12 (0.04 μM) combined with increasing concentrations of Vandetanib and the results were compared to Vandetanib and LLL12 monotherapy. The average values of triplicated experiments with the corresponding SD clearly showed an apparently synergistic effect of the two inhibitors. **D)** Western blot analysis of canonical (AKT, ERK) and non-canonical (STAT3) targets of RET signaling. Cell lysates from untreated MZ-CRC-1 cells, and those treated with increasing concentrations of Vandetanib (0.01; 0.1; 0.5 μM), 0.04 μM LLL12 and a combination of LLL12 and Vandetanib (0.04 μM and 0.1 μM, respectively) were subjected to Western blot analyses for pERK, pAKT, pSTAT3 and GAPDH (loading control). Combined treatment with sub-IC_{50} concentrations of the two drugs potentiate the inhibition of effectors of RET downstream signaling.

Figure 1.

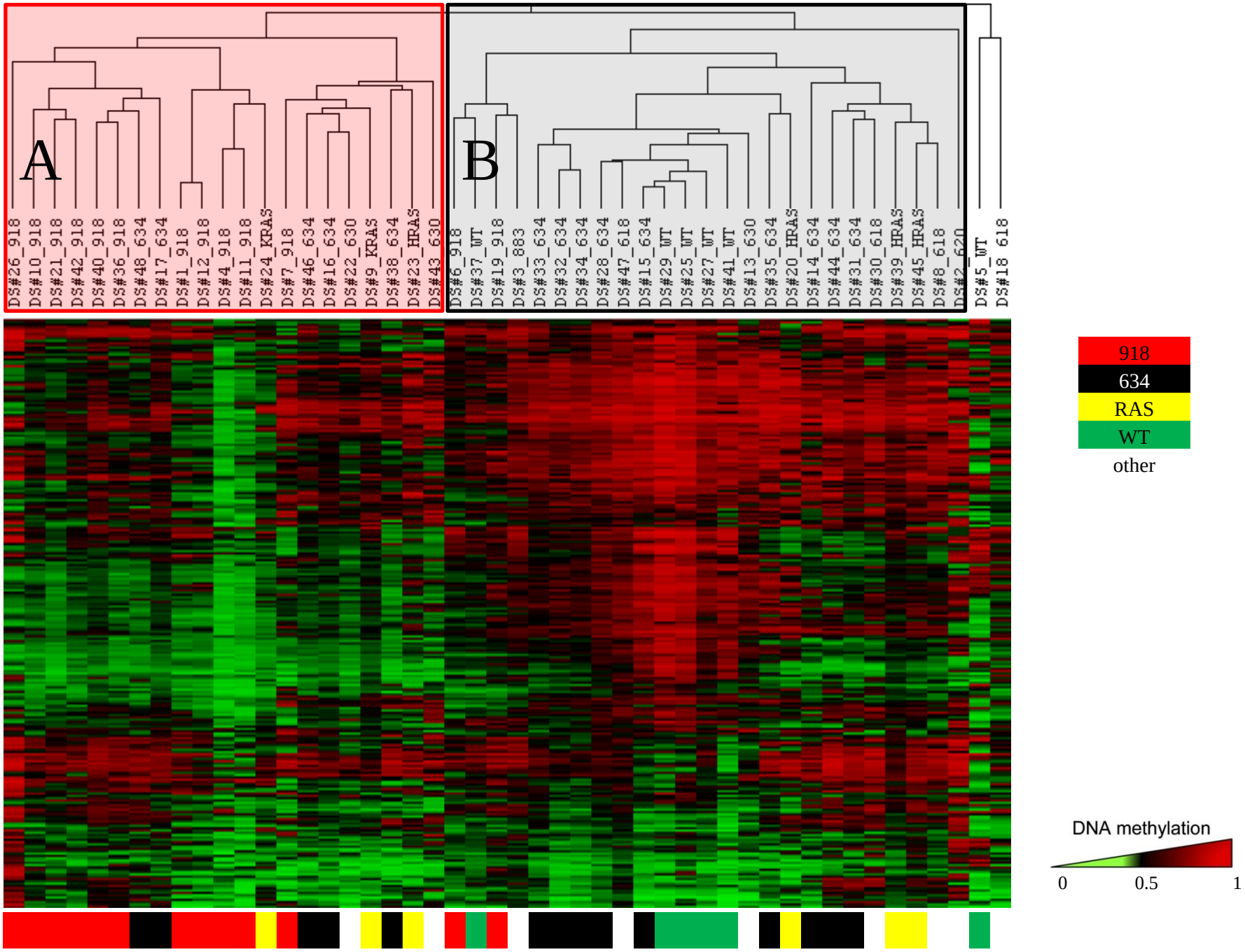
A
B
DS#26_918
DS#10_918
DS#21_918
DS#42_918
DS#40_918
DS#36_918
DS#48_634
DS#17_634
DS#1_918
DS#12_918
DS#4_918
DS#11_918
DS#24_KRAS
DS#7_918
DS#46_634
DS#16_634
DS#22_630
DS#9_KRAS
DS#38_634
DS#23_HRAS
DS#43_630
DS#6_918
DS#37_WT
DS#19_918
DS#3_883
DS#33_634
DS#32_634
DS#34_634
DS#28_634
DS#47_618
DS#15_634
DS#29_WT
DS#25_WT
DS#27_WT
DS#41_WT
DS#13_630
DS#35_634
DS#20_HRAS
DS#14_634
DS#44_634
DS#31_634
DS#30_618
DS#39_HRAS
DS#45_HRAS
DS#8_618
DS#2_620
DS#5_WT
DS#18_618
918
634
RAS
WT
other
DNA methylation
0
0.5
1

Figure 2.

A

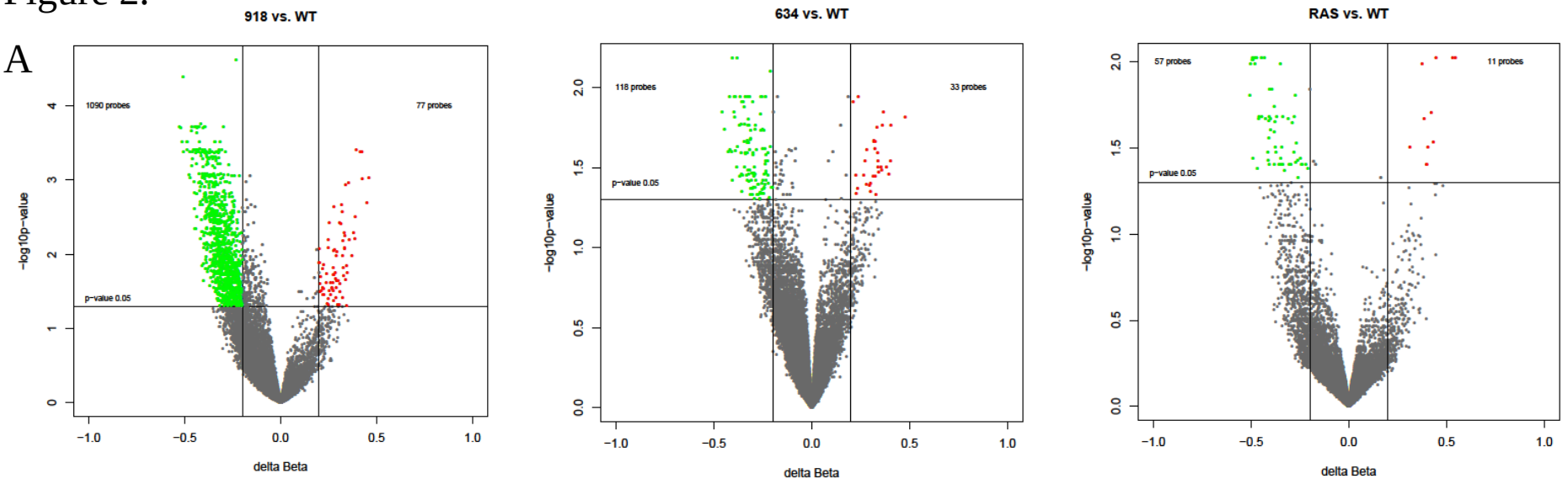
918 vs. WT
1090 probes
77 probes
p-value 0.05
−log10p-value
delta Beta
634 vs. WT
118 probes
33 probes
p-value 0.05
−log10p-value
delta Beta
RAS vs. WT
57 probes
11 probes
p-value 0.05
−log10p-value
delta Beta

B

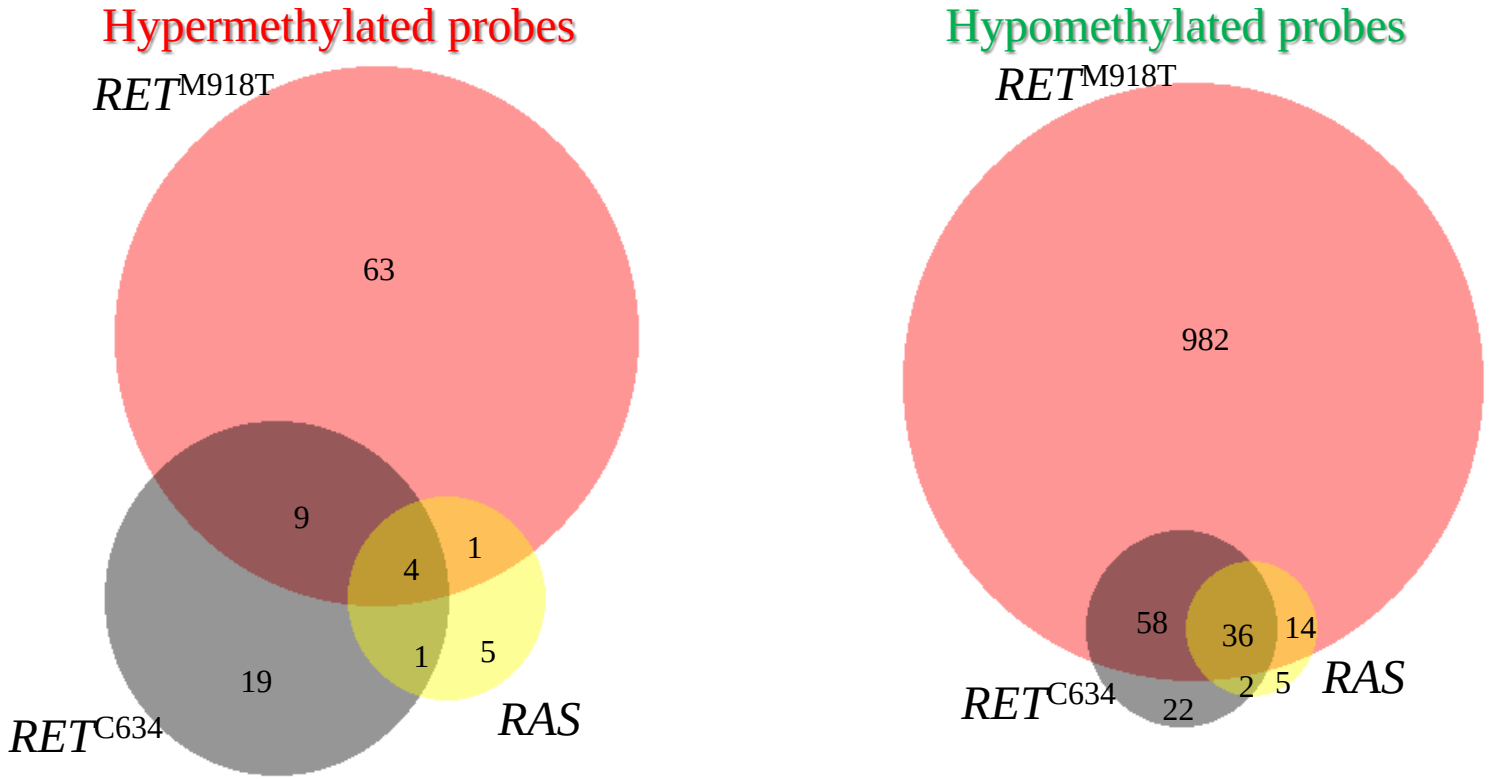
Hypermethylated probes
RETM918T
63
9
4
1
19
1
5
RETC634
RAS
Hypomethylated probes
RETM918T
982
58
36
14
2
5
22
RETC634
RAS

C

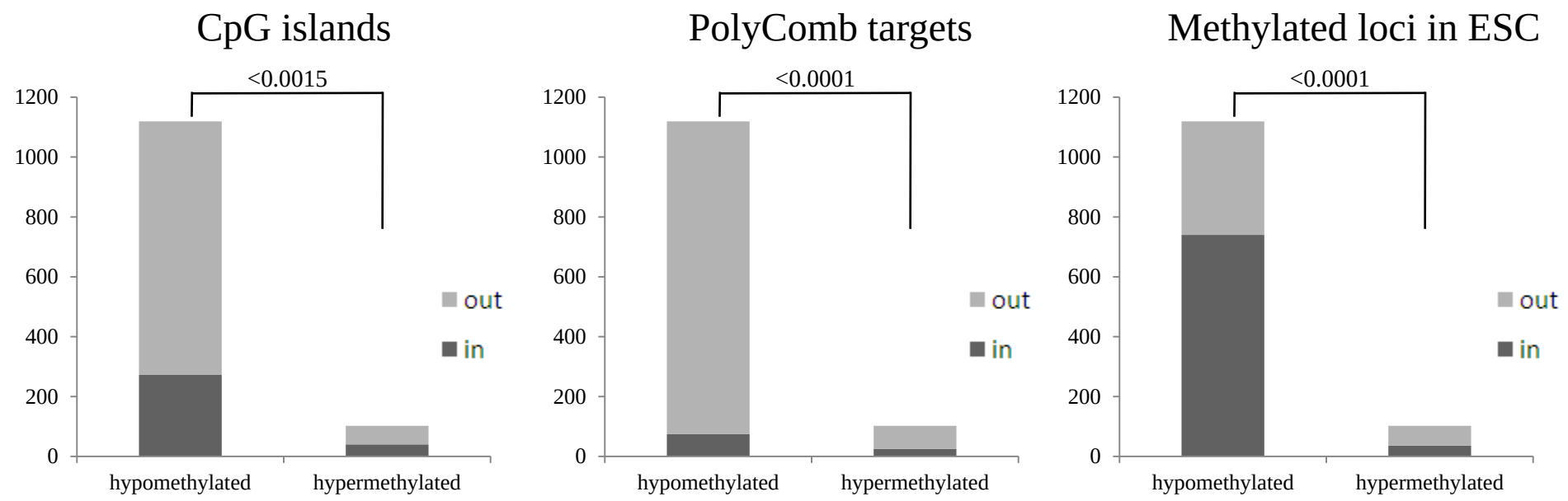
CpG islands
<0.0015
1200
1000
800
600
400
200
0
out
in
hypomethylated
hypermethylated
PolyComb targets
<0.0001
1200
1000
800
600
400
200
0
out
in
hypomethylated
hypermethylated
Methylated loci in ESC
<0.0001
1200
1000
800
600
400
200
0
out
in
hypomethylated
hypermethylated

Figure 3

A

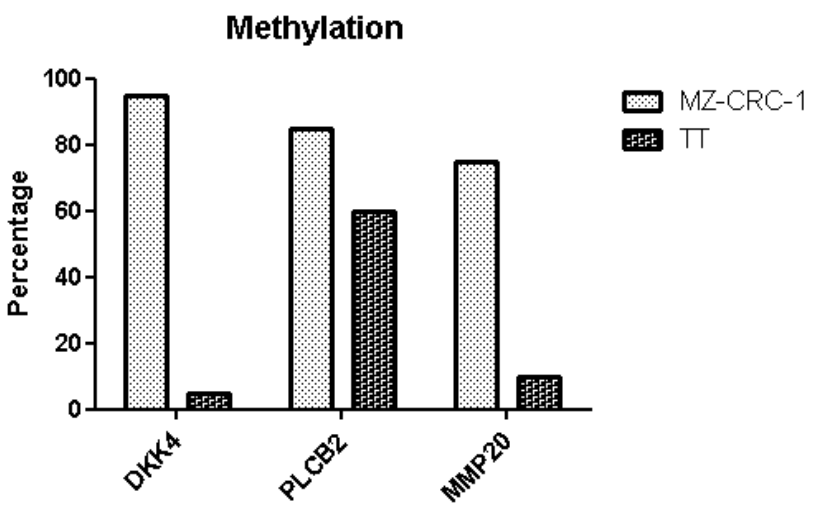
Methylation
Percentage
100
80
60
40
20
0
DKK4
PLCB2
MMP20
MZ-CRC-1
TT

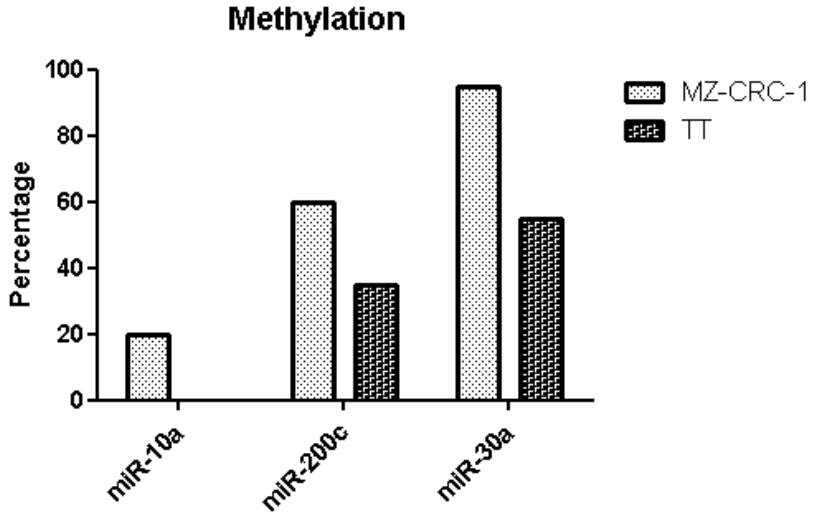
Methylation
Percentage
100
80
60
40
20
0
miR-10a
miR-200c
miR-30a
MZ-CRC-1
TT

B

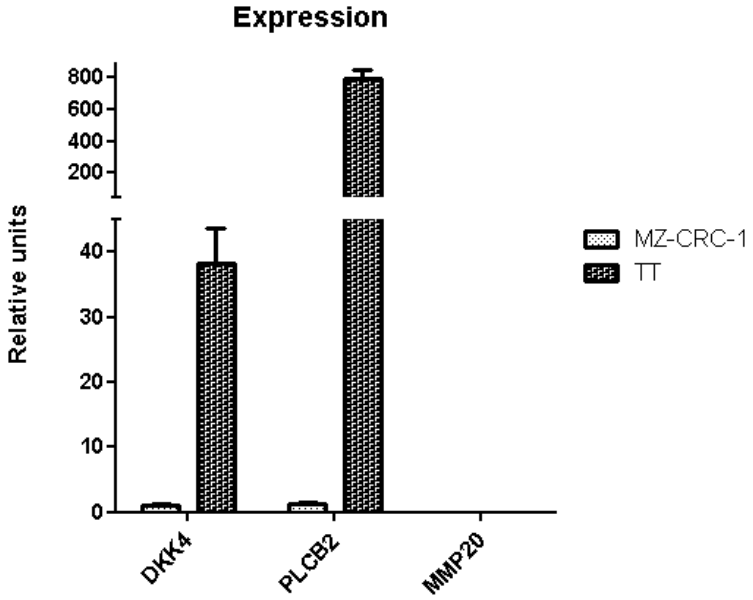
Expression
Relative units
800
600
400
200
40
30
20
10
0
DKK4
PLCB2
MMP20
MZ-CRC-1
TT

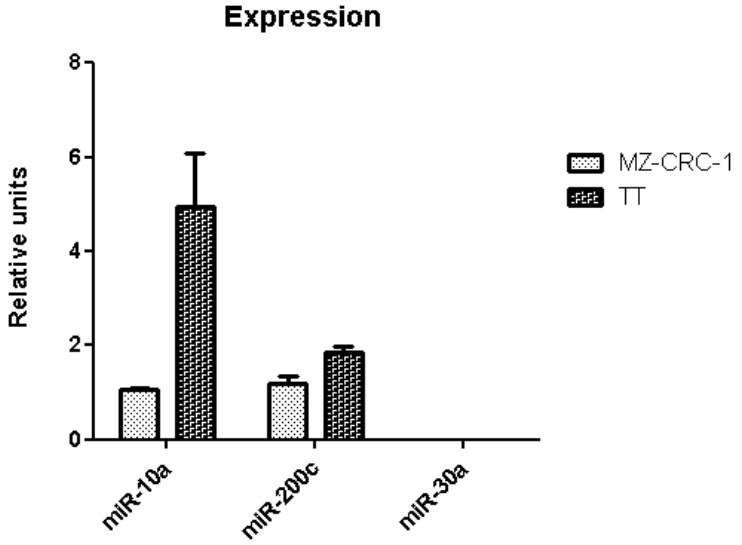
Expression
Relative units
8
6
4
2
0
miR-10a
miR-200c
miR-30a
MZ-CRC-1
TT

C

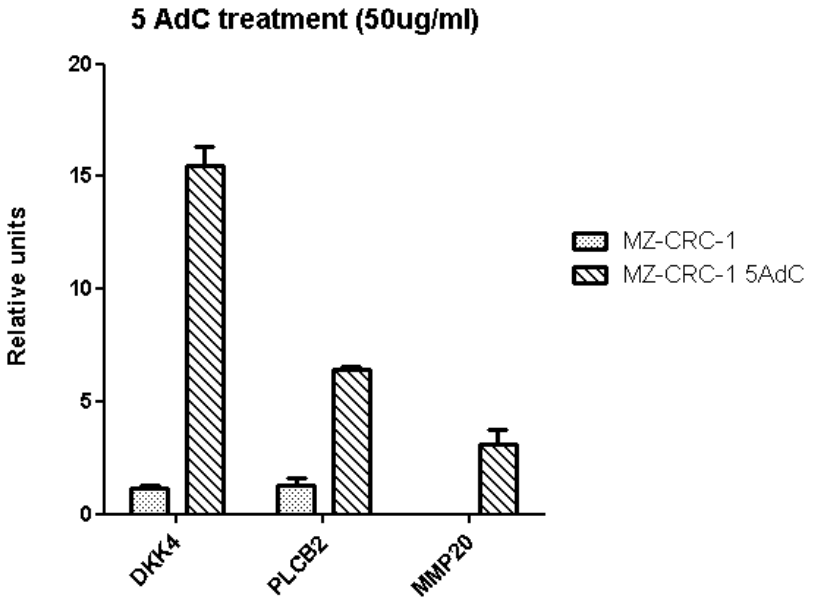
5 AdC treatment (50ug/ml)
Relative units
20
15
10
5
0
DKK4
PLCB2
MMP20
MZ-CRC-1
MZ-CRC-1 5AdC

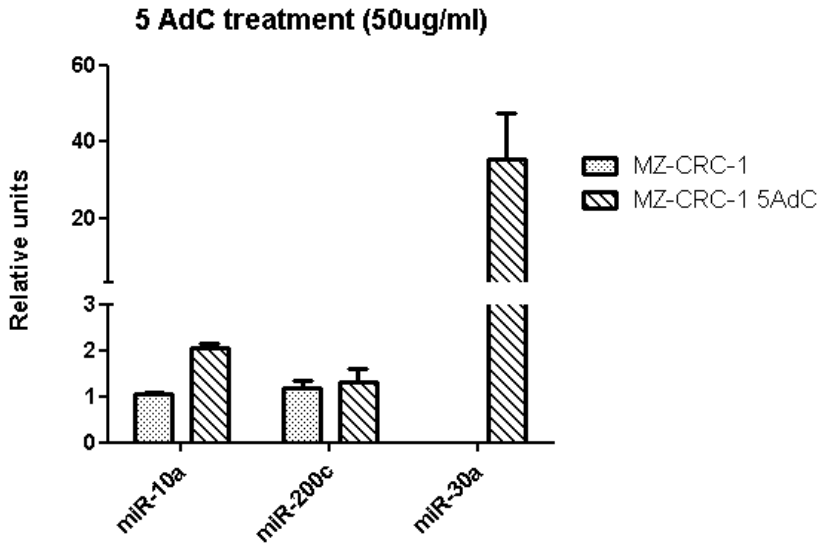
5 AdC treatment (50ug/ml)
Relative units
60
40
20
3
2
1
0
miR-10a
miR-200c
miR-30a
MZ-CRC-1
MZ-CRC-1 5AdC

Figure 4.

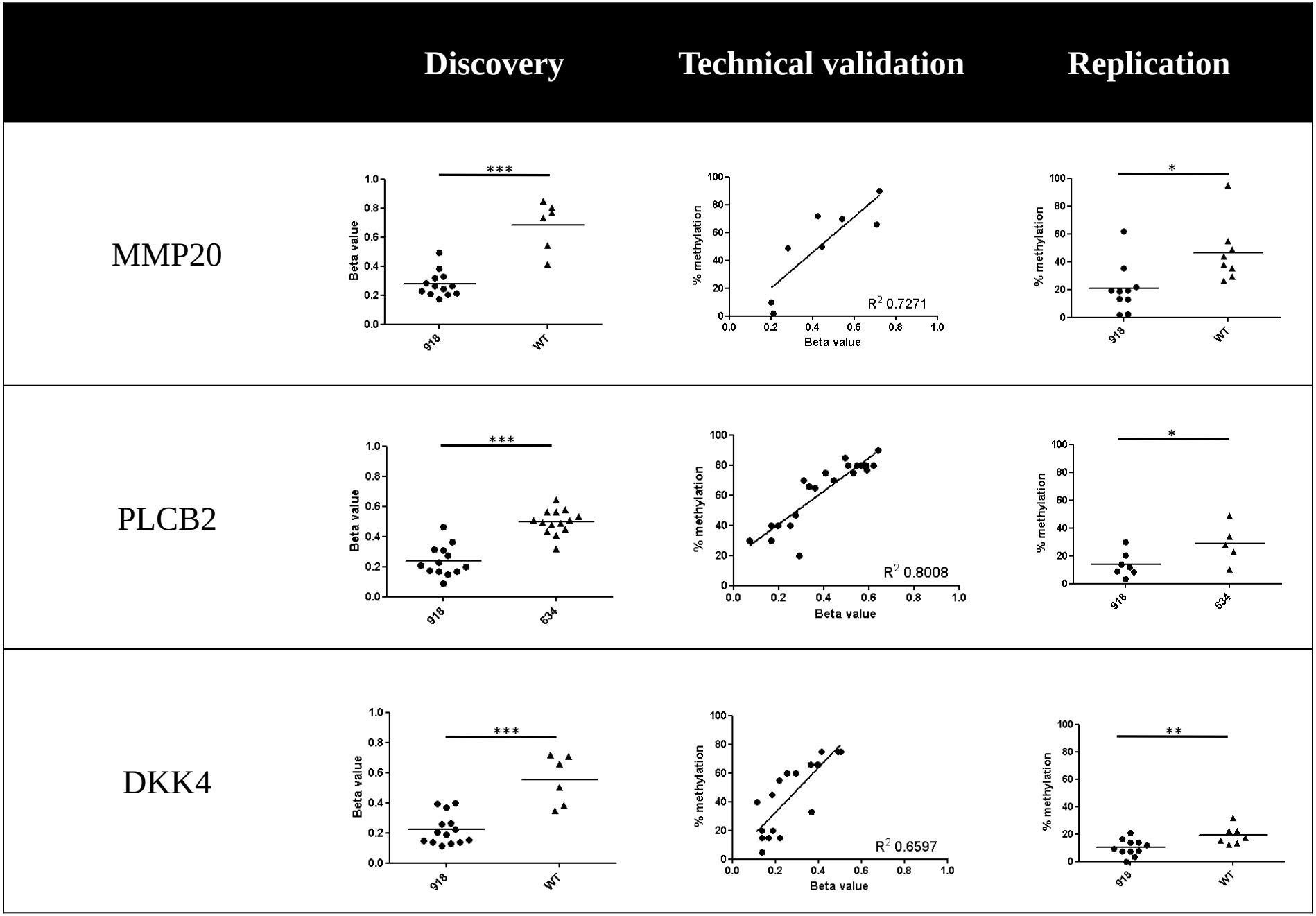

* *p*-value < 0.05; ** *p*-value < 0.01; *** *p*-value < 0.001

Figure 5

A

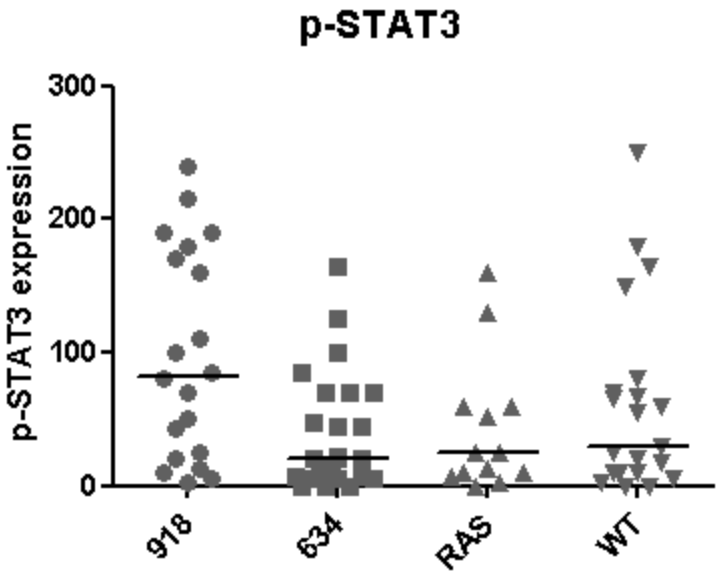

B

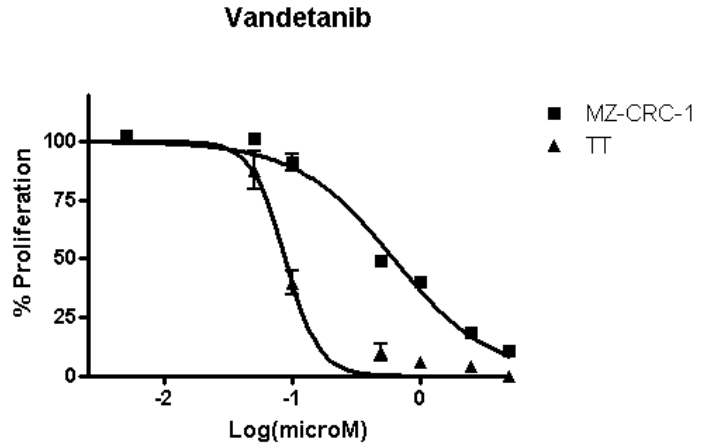

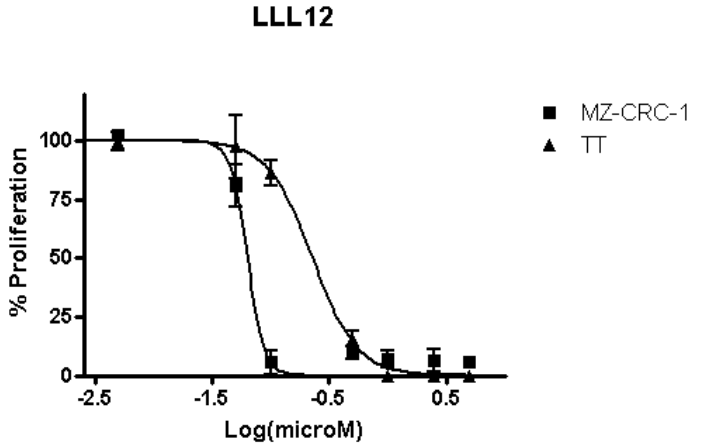

VANDETANIB	IC_{50} (μM)	95% CI (μM)
MZ-CRC-1	0.62	0.48-0.79
TT	0.09	0.05-0.16

LLL12	IC_{50}(μM)	95% CI (μM)
MZ-CRC-1	0.06	0.05-0.08
TT	0.23	0.21-0.25

C

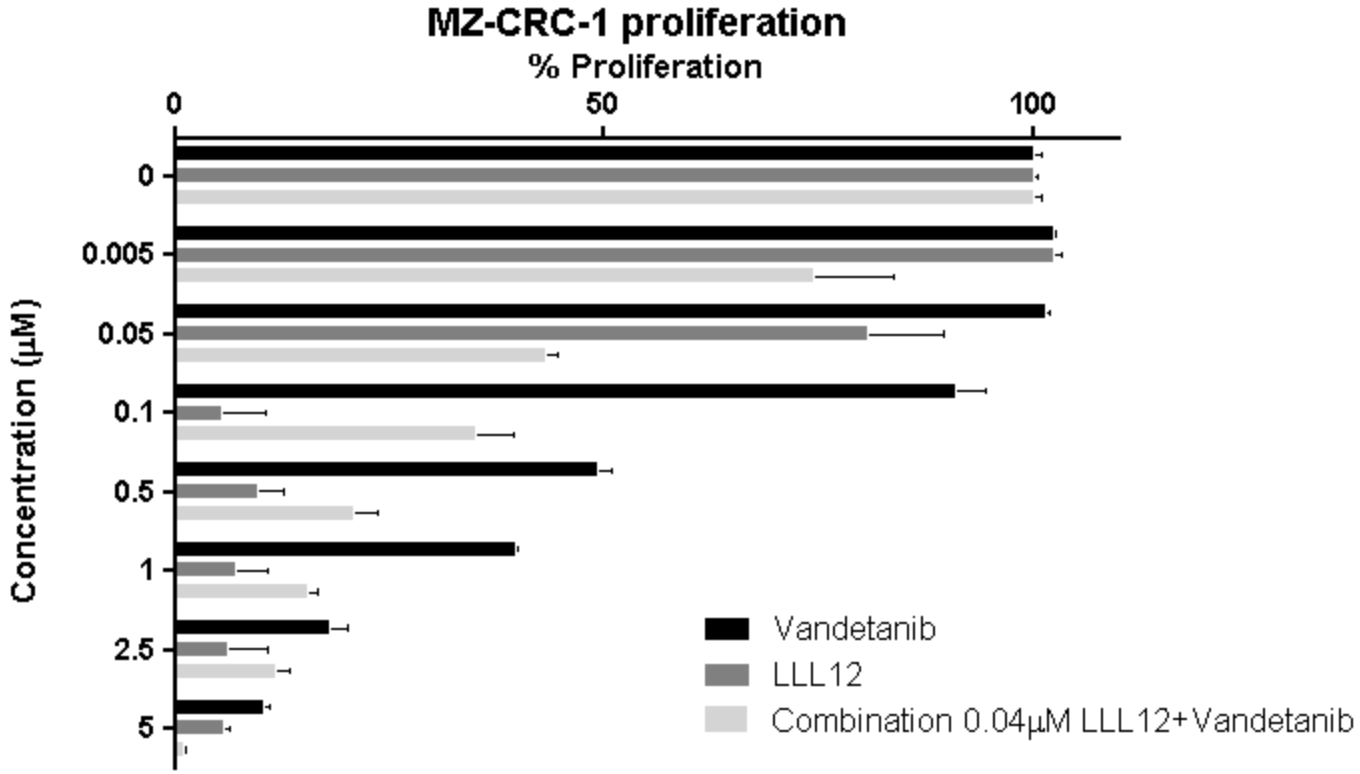
MZ-CRC-1 proliferation
% Proliferation
0
50
100
Concentration (μM)
0
0.005
0.05
0.1
0.5
1
2.5
5
Vandetanib
LLL12
Combination 0.04μM LLL12+Vandetanib

D

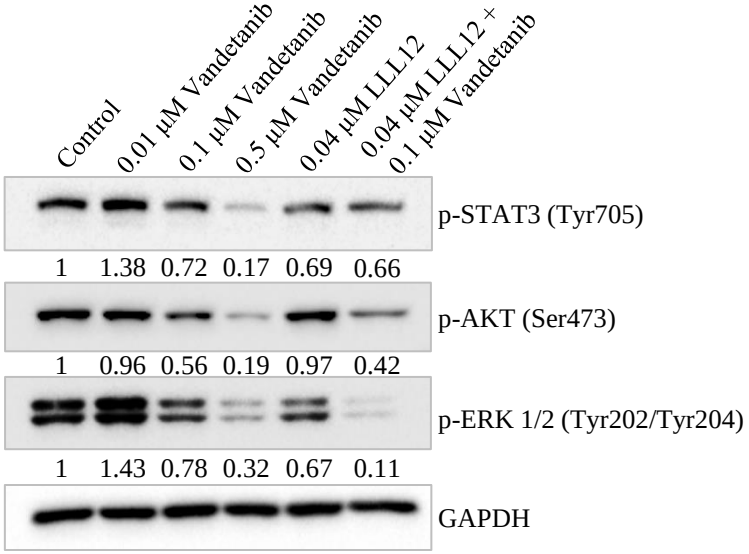
Control
0.01 μM Vandetanib
0.1 μM Vandetanib
0.5 μM Vandetanib
0.04 μM LLL12
0.04 μM LLL12 + 0.1 μM Vandetanib
p-STAT3 (Tyr705)
1 1.38 0.72 0.17 0.69 0.66
p-AKT (Ser473)
1 0.96 0.56 0.19 0.97 0.42
p-ERK 1/2 (Tyr202/Tyr204)
1 1.43 0.78 0.32 0.67 0.11
GAPDH